A numerical model and scaling relationship for energetic electron beams propagating in air

R. F. Fernsler,[1,a)] S. P. Slinker,[1] and S. G. Lambrakos[2]
[1]*Plasma Physics Division, Naval Research Laboratory, Washington, DC 20375, USA*
[2]*Materials Science and Technology Division, Naval Research Laboratory, Washington, DC 20375, USA*

(Received 6 June 2008; accepted 4 August 2008; published online 30 September 2008)

Scaling relationships for energy loss and scattering are combined with a particle code to construct a purely algebraic expression for the energy deposited by an energetic electron beam injected into field-free homogeneous air. An algebraic formulation is possible because the mean free paths for the major collisional processes depend similarly on density and energy above 1 keV. Accordingly, the spatial behavior of an initially cold pencil beam is approximately self-similar when expressed in terms of the nominal beam range, provided the beam energy at injection exceeds several keV. Since a warm and broad beam can always be decomposed into a series of cold pencil beams, the total energy deposited can be obtained through a simple sum. With such a model, the ionization and excitation generated by a beam can be computed quickly and easily at every point in space. Similar formulations can be developed for other media using particle codes or experimental data. In liquids or solids, the energy deposited is quickly converted to heat and ultimately to melting and/or vaporization of the material. [DOI: 10.1063/1.2986657]

I. INTRODUCTION

The advance of energetic electrons through a medium has been studied for well over 50 years[1] and is of interest for a wide range of problems. These problems include radiation effects on biological systems,[2] optical emissions in the upper atmosphere,[3–5] electron-beam pumping of lasers,[6–9] pollution remediation,[10] fluorescence diagnostics,[11] beam-produced plasmas for materials processing[12–14] and radar applications,[15] and welding, bonding, cutting, annealing, hardening, and fabrication of solid materials.[16] The energy deposited by the beam is the primary parameter of interest in all of these applications. Modeling the advance of a beam is difficult because collisions with the background molecules deflect as well as extract energy from the beam electrons.[1,17] Boltzmann calculations[7,8,18] have been widely used and give the electron energy distribution but not the spatial distribution. An alternative and more complete approach is to follow the beam electrons as particles and treat collisions using a Monte Carlo method.[9,14,19–23] However, large numbers of particles must be used to obtain smooth and accurate results over the entire beam range. Exploring a wide set of parameters is thus costly,[17,19] especially for beams that are noncylindrical and inherently three-dimensional.

In this work we describe an approach that is potentially far simpler, faster, and cheaper. The approach is justified provided that (i) the initial beam energy is several keV or more, (ii) self-forces and external forces are negligible, and (iii) the primary collision targets are ground-state molecules. The electron collision rates are then proportional to the molecular density N, while the distance between collisions is proportional to $1/N$. Although the dependence on energy is more complicated,[24,25] it is similar for the largest rates above 1 keV. The major ionization and excitation rates are therefore nearly directly proportional to one another, and these rates largely determine the electron energy distribution and the rate at which the beam loses energy. These properties lead to two conclusions. First, the ionization and excitation rates are almost directly proportional to the beam energy being deposited at each point in space. Second, because the mean free paths for both elastic and inelastic scatterings vary similarly with density and energy, a common collisional scale length governs much of beam behavior. Accordingly, the energy deposited by an initially cold pencil beam can be expressed in a nearly self-similar form,

$$\frac{dE_b}{dt} = \frac{I_b V_b}{R^3} f(r/R, \theta). \tag{1}$$

Here I_b is the injected beam current, V_b is the beam voltage, R is the nominal beam range, r is the distance from the point of injection, θ is the angle with respect to the axis of injection, and $f(r/R, \theta)$ is a nearly universal dimensionless function for a given medium (see Fig. 1). Although energy deposition is the focus of the present analysis, the self-similar formulation can be used to predict other beam parameters as well.

The range R depends on both V_b and the molecular density N of the medium. Once $R(V_b, N)$ and $f(r/R, \theta)$ have been determined, the energy deposited by any energetic beam can be easily estimated, since a warm and broad beam can always be decomposed into a series of cold pencil beams. Adding the contributions of the pencil beams gives the energy deposited by the full beam. Moreover, the local ionization and excitation rates are easily obtained from the beam energy being deposited. In dense media, the absorbed energy is trapped and thus soon goes into heating and ultimately into melting or vaporization of the material.

Experiments on light emission support the above predictions over a limited range in energy.[22,26–28] However, no at-

[a)]Electronic mail: richard.fernsler@nrl.navy.mil.

Downloaded 02 Oct 2008 to 132.250.158.10. Redistribution subject to AIP license or copyright; see http://jap.aip.org/jap/copyright.jsp

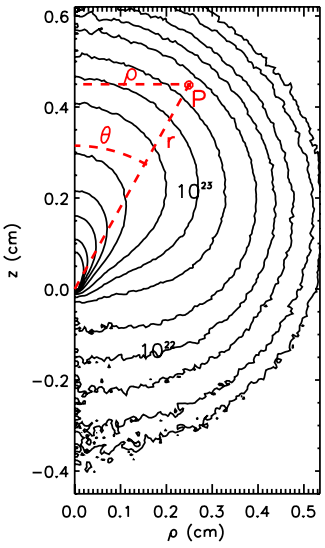

FIG. 1. (Color online) An electron beam propagates upward in z through 100 torr of nitrogen, starting from the origin (0,0). The beam was injected warm and had an initial energy of 5 keV, a current of 1 A, and a radius of 1 mm. Contours of the energy-deposition rate are plotted in intervals of $1\times10^{22}-1\times10^{27}$, $2\times10^{22}-2\times10^{27}$, and $5\times10^{22}-5\times10^{27}$ eV/cm^3 s. The location of any point P can be expressed (dashed red lines) either as (ρ,z) or (r,θ), where z is the distance along the beam axis, ρ is the distance from the axis, $r=(\rho^2+z^2)^{1/2}$ is the total distance from the injection point, and $\theta=\sin^{-1}(\rho/r)$ is the polar angle.

tempt was made to fit $f(r/R,\theta)$ algebraically, and the importance of elastic scattering, which controls the lateral spread of the beam, was not fully appreciated. In addition, some authors gave undue importance to the form of the excitation cross sections, and none of the experiments held a_0/R rigorously constant, as required by self-similarity; here a_0 is the beam radius at injection. Pencil beams $(a_0\rightarrow0)$ satisfy the latter condition automatically, of course.

Early attempts to compute energy deposition were only partially successful.[17] For example, Lewis[29] used the continuous-slowing-down approximation to treat energy loss and then derived an integrodifferential diffusion equation in units of R to treat elastic scattering. However, no attempt was made to solve this equation. Spencer[17] attempted to solve the equation numerically, but particle codes are simpler and more straightforward to use. In addition, while separating energy loss from scattering is useful, it obscures the fact that these processes depend similarly on energy, so the self-similar nature of the solutions was not fully recognized. Last, the models fail far from the source because the continuous-slowing-down approximation precludes range straggling.[17]

Both the earlier models and the present model strictly apply only in homogeneous media without boundaries. However, as will become evident, these models are often sufficient even when boundaries are present because backscattering and reflection are weak. Indeed, in the aforementioned experiments, the electron beam emerged from behind a solid plane, yet the light emitted from the gas remained approximately self-similar and in good agreement with results obtained herein. Recall too that the self-similar assumption is only an approximation even without boundaries.

To illustrate the concept and determine R and $f(r/R,\theta)$, we constructed a particle code to model electron beams propagating in air. The code uses a set of discrete cross sections in nitrogen and oxygen and follows both the beam electrons and the daughter electrons created by ionization. The daughter electrons are followed because they are ejected mainly transverse to the beam and thus broaden the volume over which energy is deposited. The run time is directly proportional to the number of daughter electrons and hence to V_b. We therefore restricted V_b to 200 kV or less. A nonrelativistic treatment was used for simplicity, but the results for $f(r/R,\theta)$ should apply at much higher energies as well, provided R is properly computed. However, at very high energies (above 100 MeV in air), bremsstrahlung becomes the dominant energy loss,[25] so the character of $f(r/R,\theta)$ changes. Figure 1 shows a contour plot of the energy deposited in a plane passing through the origin for a beam injected with 5 keV and 1 A into 100 torr of nitrogen. These contours closely resemble those measured optically by Cohn and Caledonia.[27]

II. NUMERICAL MODEL

In this section we describe the particle code PLUME used to determine the steady-state behavior of an electron beam passing through air consisting of 80% nitrogen and 20% oxygen. The code follows both the beam electrons and the daughter electrons created by ionization, and it also gives the major ionization and excitation rates. The rates are obtained by injecting a large number of beam electrons with specified initial positions and velocities. Collisions with air molecules are treated using a Monte Carlo approach. To minimize the run time, each electron is followed until its energy falls below some minimum value, $\varepsilon_{\min}$. Electrons with energies below $\varepsilon_{\min}$ are treated separately using fluid equations not described here. Because elastic collisions strongly confine low-energy electrons and because ionization ceases below 12 eV in air, we set $\varepsilon_{\min}$ to 10 eV in this work. The run time increases significantly if $\varepsilon_{\min}$ is reduced. The production rates are computed by dividing the simulation space into volume elements and then determining the number of ions or excited molecules produced in each element. Those numbers are divided by the volume of each element and by the number of beam electrons launched. Multiplying these values by the beam current gives the volumetric production rates for any beam having the same initial configuration in space, energy, and temperature. Self-forces are ignored although external electric and magnetic fields can be added if desired.

In order to model collisions, the air molecules are assumed to be cold in the ground state and of uniform density N. Because energetic electrons suffer hundreds of collisions or more before reaching $\varepsilon_{\min}$, the collisions are treated stochastically using a set of differential cross sections, $d\sigma_{jk}/d\Omega$, where the subscript j identifies the type of collision suffered and k refers to the molecule type (N_2 or O_2). The probability that a particular collision deflects an electron with energy ε through an angle greater than θ is given by

Downloaded 02 Oct 2008 to 132.250.158.10. Redistribution subject to AIP license or copyright; see http://jap.aip.org/jap/copyright.jsp

$$P_{jk}(\varepsilon,\theta)=\frac{\int_{-1}^{\cos\theta} d(\cos\theta')\frac{d\sigma_{jk}(\varepsilon,\theta')}{d\Omega}}{\int_{-1}^{1} d(\cos\theta')\frac{d\sigma_{jk}(\varepsilon,\theta')}{d\Omega}}. \tag{2}$$

The Monte Carlo method uses this relationship to assign random numbers between zero and unity to P_{jk} for each type of collision. The deflection angles $\theta(P_{jk},\varepsilon)$ suffered during a time Δt are then chosen based on the random numbers P_{jk} and the collision probabilities $\nu_{jk}(\varepsilon)\Delta t$, where the frequency of a particular type of collision is given by

$$\nu_{jk}(\varepsilon)=2\pi n_k\sqrt{\frac{2\varepsilon}{m}}\int_{-1}^{1} d(\cos\theta')\frac{d\sigma_{jk}(\varepsilon,\theta')}{d\Omega}. \tag{3}$$

Here m is the electron mass and n_k is the density of scattering centers for neutral species k. To minimize the probability that an electron suffers more than one collision during Δt, the time step is constrained to $\Delta t \leq 0.1/\nu_{\max}$, where $\nu_{\max}$ is the maximum collision frequency for $\varepsilon \geq \varepsilon_{\min}$. Given this choice, "null" collisions occur far more frequently than actual collisions.

Collisions come in three general classes. Elastic collisions occur most often and mainly scatter the beam. The mean deflection per collision is small but the cumulative deflection is not. Once the scattering angle becomes large, the electrons no longer advance as a beam but diffuse in all directions instead. Because the beam energies being considered are modest ($\leq$200 keV), the total number of collisions suffered is sufficiently small that each collision can be treated individually. The "condensed history technique" widely employed in other codes[19,20] is thus not used.

Elastic collisions favor forward scattering at high energy but isotropic scattering at low energy. To allow for that change, we treated elastic collisions using the Rutherford cross section in a form first described by Moliere.[30] This form can be written as

$$\frac{d\sigma_{\rm el}^{(k)}}{d\Omega}=\left(\frac{Z_k e^2}{mu^2}\right)^2\frac{1}{(1-\cos\theta+2\eta_k)^2}, \tag{4}$$

where u is the electron velocity, $Z_k e$ is the nuclear charge of molecular species k, and $-e$ is the electron charge. The energy-dependent factor η_k is added both to make the differential cross section isotropic at low energy and to keep the total cross section finite,

$$\sigma_{\rm tot}^{(k)}=\int d\Omega\frac{d\sigma_{\rm el}^{(k)}}{d\Omega}=\left(\frac{Z_k e^2}{mu^2}\right)^2\frac{\pi}{\eta_k(1+\eta_k)}. \tag{5}$$

Inserting Eq. (4) into Eq. (2) and inverting the result, we find that the deflection caused by elastic collisions can be assigned a value,

$$\theta(P_k,\varepsilon)=\cos^{-1}\left[1+2\eta_k-\frac{2\eta_k(1+\eta_k)}{\eta_k+P_k}\right], \tag{6}$$

where P_k is a random number between zero and unity.

The form used for $d\sigma_{\rm el}/d\Omega$ is unimportant provided[31] it preserves both the momentum-transfer cross section σ_m and the total elastic cross section $\sigma_{\rm tot}$. Thus η_k was chosen to do just that. Specifically, we first used Eqs. (4) and (5) to relate σ_m to $\sigma_{\rm tot}$,

$$\sigma_m^{(k)}\equiv 2\pi\int_{-1}^{1} d(\cos\theta)(1-\cos\theta)\frac{d\sigma_{\rm el}^{(k)}}{d\Omega}$$
$$=2\eta_k\left[(1+\eta_k)\ln\left(\frac{1+\eta_k}{\eta_k}\right)-1\right]\sigma_{\rm tot}^{(k)}. \tag{7}$$

We then obtained a fit for η_k using values given by Mayol and Salvat[31] for $\sigma_m/\sigma_{\rm tot}$ in atomic nitrogen ($Z_k=7$) as a function of energy. The result was

$$\eta_k \simeq 1.17\times 10^{-5}\frac{Z_k^{2/3}}{\gamma^2-1}, \tag{8}$$

where $\gamma=1+\varepsilon/mc^2$ is the relativistic mass factor and mc^2 is the electron rest energy. The same fit was used for oxygen ($Z_k=8$), and it differs only slightly from Moliere's result[30] as reported by Jackman and Green.[32] Okhrimovsky *et al.*[33] obtained a different fit at low energy, but at low energy the electron range is so short that the fit used for η_k no longer matters. To compute the elastic collision frequency, we used values for $\sigma_{\rm tot}$ from Mayol and Salvat[31] at energies above 1 keV and from Itikawa *et al.*[34,35] at energies below 1 keV. The energy transferred to the molecule was then computed using conservation of momentum and energy. This loss is negligible, however, compared to the energy consumed by inelastic collisions.

Electronic excitation is the second class of collision, and in this case the excitation energy determines the energy loss. The code results that will be presented later are based on 36 discrete excited states for nitrogen and 15 states for oxygen. For representative states and cross sections, see Refs. 18 and 36. The cross section for an optically allowed (dipole) transition from the ground state to an excited state j for neutral species k is written as[7,37]

$$\sigma_{jk}(\varepsilon)=A_{jk}\left(\frac{\varepsilon-E_{jk}}{\varepsilon^2}\right)\ln\left(\frac{\gamma^2\varepsilon e^{-\beta^2}}{w_{jk}}\right). \tag{9}$$

Here $\varepsilon=mu^2/2$ is the electron energy immediately prior to colliding, A_{jk} is a constant, E_{jk} is the excitation energy, w_{jk} is a scale energy, $\beta=u/c$ is the relativistic velocity factor, and e is the base of the natural logarithm. Equation (9) remains valid even as $u\to c$. The cross sections for optically forbidden states (metastables) have a different dependence on energy,[7,36] but they are much smaller than the ionization cross sections above 1 keV. Thus, although the forbidden states are included in PLUME, they extract little energy from the beam and are therefore ignored in the analytic model that will be presented later. Because the code does not include all states, the values for w_{jk} were adjusted until the energy loss function $d\varepsilon/ds$ had a similar dependence on ε as predicted by the Born-Bethe model.[38]

The differential cross sections for excitation are not well known, so angular deflection was computed as follows. Because the incident electron repels the orbital electron both on coming and going, the orbital electron mainly receives a sideways kick. Both electrons therefore experience a change

Downloaded 02 Oct 2008 to 132.250.158.10. Redistribution subject to AIP license or copyright; see http://jap.aip.org/jap/copyright.jsp

in transverse momentum given by $\Delta p_\perp \simeq (2mE_{jk})^{1/2}$, and consequently the incident electron is deflected through an angle

$$\theta_{jk} \simeq \sin^{-1}\left(\frac{\Delta p_\perp}{p}\right) \simeq \sin^{-1}\left(\sqrt{\frac{E_{jk}}{\varepsilon}}\right). \tag{10}$$

Here $p=mu$ is the momentum of the incident electron immediately prior to colliding. Equation (10) is strictly valid only for energies $\varepsilon \gg E_{jk}$, but at low energy the electron range is so short that deflection is unimportant. Furthermore, the deflection from excitation is negligible compared to that produced by elastic scattering.

Ionization is the third class of collision, and it accounts for most of the energy lost by energetic beams. The cross sections for ionization take the same form as Eq. (9), but during ionization one or more secondary electrons are created. The energy lost by the incident electron thus equals the ionization energy E_{jk} of the molecule plus the kinetic energy ε_s imparted to the secondaries. The secondary energy ε_s was chosen using a distribution of the form $f_i(\varepsilon_s) \propto (\varepsilon_s^2+\varepsilon_k^2)^{-1}$ based on measurements by Opal *et al.*[39] Here $\varepsilon_k \sim E_{jk}$ is another scale energy for gas species k. To specify the deflection angles, we assumed that the ion absorbs the potential energy E_{jk} but acquires no kinetic energy. The primary and secondary electrons then absorb the initial momentum as well as any excess energy, and consequently the primary electron is deflected through an angle

$$\theta_p = \cos^{-1}\left(\frac{\varepsilon_p + E_{jk}/2}{\sqrt{\varepsilon_p \varepsilon}}\right). \tag{11}$$

Similarly the secondary electron leaves at an angle

$$\theta_s = \cos^{-1}\left(\frac{\varepsilon_s + E_{jk}/2}{\sqrt{\varepsilon_s \varepsilon}}\right). \tag{12}$$

Here $\varepsilon_p \geq \varepsilon_s$ is the energy of the primary after ionization and ε is its energy before ionization. Not surprisingly, Eq. (11) yields the same result as Eq. (10) when $\varepsilon_s=0$. The predictions for θ_s from Eq. (12) agree well with the peak in the double-differential cross sections computed by Manson *et al.*[40] and measured by Opal *et al.*[39] The neglect of ion momentum is strictly justified only if $\varepsilon > 2E_{jk}$ and $\varepsilon_s > E_{jk}^2/4\varepsilon$, but fortunately deflection is unimportant at low energy. Note too that θ_p is generally small whereas θ_s is usually close to 90°. Most secondaries are therefore ejected nearly perpendicular to the beam, thus broadening the volume over which energy is deposited.

After running the code, the mean energy ε_{jk} for each state was computed by dividing the total beam energy at injection by the number of ionized or excited molecules created. As is well known,[41] the mean energies ε_{jk} are independent of the gas density N and are insensitive to the initial beam energy ε_0, and indeed the values listed in Table I varied by less than 5% for $5 \leq \varepsilon_0 \leq 200$ keV. The values for ε_{jk} also varied little with position from well behind the beam to far in front. The spatial variation is weak because low-energy electrons have such a short mean free path that they exist only where high-energy electrons are present to create them. Accordingly, the electron energy distribution retains a high-energy tail even far from the source. Equally important, ε_{jk} is approximately constant for states having cross sections different from Eq. (9), provided those cross sections fall off at least as rapidly with ε. In all cases the local production rates equal the energy-deposition rate divided by ε_{jk}, while the production efficiencies equal the threshold energy E_{jk} divided by ε_{jk}.

TABLE I. Threshold energies E_{jk} and mean energies ε_{jk} for the key ions in air. The mean energies varied by less than 5% for initial beam energies between 5 and 200 keV. The mean energy $\bar{\varepsilon}_i$ per ion pair represents an average taken over all ionization states, and it varied by less than 5% down to initial energies as low as 1 keV.

Species	E_{jk} (eV)	ε_{jk} (eV)
$N_2^+(X)$	15.6	130
$N_2^+(A)$	16.6	120
$N_2^+(B)$	18.8	375
$N_2^+(F^2\Sigma)$	27.5	2820
$N_2^+(\sigma_g 2s)$	35.0	295
N_2^{2+}	42.5	1850
$O_2^+(X)$	12.06	830
$O_2^+(a)$	16.1	460
$O_2^+(A)$	16.9	2020
$O_2^+(b)$	18.2	1225
$O^+ + O$	19.0	500
		$\bar{\varepsilon}_i = (\Sigma \varepsilon_{jk}^{-1})^{-1} = 34$

III. ANALYTIC MODEL

As indicated by Eq. (9), the major inelastic cross sections all have a similar form, and therefore the coefficient for energy absorption is well represented by

$$\mu_\varepsilon(N,\varepsilon) \equiv -\frac{1}{\varepsilon}\frac{d\varepsilon}{ds} = \frac{1}{\varepsilon}\sum_{j,k} N_k E_{jk} \sigma_{jk}(\varepsilon) \simeq \frac{B_{\text{in}} N \ln(\varepsilon/I_{ex})}{\varepsilon^2}. \tag{13}$$

Here ds is an element of path length, N_k is the number density of species k, $N=\Sigma N_k$ is the total molecular density, $B_{\text{in}} = \Sigma (N_k/N) A_{jk} E_{jk}$ is a constant, I_{ex} is a weighted average[38] of w_{jk}, and the relativistic factors γ and β have been dropped for convenience. Note that the energy loss function $d\varepsilon/ds$ varies as $\ln(\varepsilon)/\varepsilon$ to lowest order. Approximation (13) applies only for energies $\varepsilon \gg E_{jk}$, and it applies over most of the beam range only if the initial beam energy ε_0 is much larger yet. Initial energies of several keV or more are thus needed for the present model to apply. Treating the logarithm in Eq. (13) as constant and integrating, the mean inelastic range is given approximately by

$$R \simeq \frac{\varepsilon_0^2}{2B_{\text{in}} N \ln(\varepsilon_0/I_{ex})}. \tag{14}$$

In contrast to inelastic collisions, elastic collisions deflect the electrons but extract little energy. Since the elastic collisions account for most of the scattering, Eqs. (5), (7), and (8) indicate that the coefficient for angular scattering is well represented by

Downloaded 02 Oct 2008 to 132.250.158.10. Redistribution subject to AIP license or copyright; see http://jap.aip.org/jap/copyright.jsp

$$\mu_s(N,\varepsilon) \equiv \sum_k n_k \sigma_m^{(k)} \simeq \frac{\pi}{2}\sum_k \left\{ \left(\frac{Z_k e^2}{\varepsilon}\right)^2 n_k \left[\ln\left(\frac{1+\eta_k}{\eta_k}\right) - \frac{1}{1+\eta_k} \right] \right\} \simeq -\frac{B_{\rm el} N \ln(\varepsilon/I_{\rm el})}{\varepsilon^2} \tag{15}$$

for energies $\varepsilon \simeq 3Z_k^{2/3}\eta_k^{-1} \gg I_{\rm el}$. Here $I_{\rm el} \simeq 8\bar{Z}^{2/3}$ is another scale energy in eV, $\bar{Z}$ is the mean atomic number, and $B_{\rm el} = (\pi/2)e^4\Sigma(n_k/N)Z_k^2$. Like Eq. (13), Eq. (15) can be used to define an effective elastic range,

$$R_{\rm el} \equiv \frac{1}{\mu_s(N,\varepsilon_0)} \simeq \frac{\varepsilon_0^2}{B_{\rm el} N \ln(\varepsilon_0/I_{\rm el})}. \tag{16}$$

The elastic range $R_{\rm el}$ represents the distance needed for the electrons to isotropize.

Equations (13)–(16) demonstrate that energy loss and scattering depend similarly on the number density N of the medium and the instantaneous electron energy ε, and this is true for most of the life of an electron provided it starts with an initial energy of several keV or more. A common collisional scale length therefore governs much of the behavior of energetic beams. Because the inelastic range R is commonly tabulated,[38] we use it as a scale length rather than the elastic range $R_{\rm el}$. Accordingly, the energy deposited by an initially cold pencil beam can be expressed as stated in Eq. (1),

$$\frac{dE_b}{dt} = \frac{I_b V_b}{R^3} f(r/R,\theta).$$

Here I_b is the injected beam current, $eV_b = \varepsilon_0$ is the initial beam energy, R is the inelastic beam range, r is the distance from the point of injection, θ is the angle with respect to the axis of injection, and $f(r/R,\theta)$ is a nearly universal scale function for a given medium. Since all of the beam energy is ultimately absorbed, the scale function $f(r/R,\theta)$ satisfies the normalization relationship,

$$R^{-3}\int d(\mathrm{vol}) f(r/R,\theta) = 1. \tag{17}$$

Beams of finite width and temperature can be treated by decomposing them into a series of pencil beams, each having a specified initial position, orientation, current, and energy. Given $f(r/R,\theta)$ and R, the energies deposited by the pencil beams can be added to determine the energy deposited by the full beam. The problem thus reduces to determining $f(r/R,\theta)$ and R for a given medium. A particle code or equivalent is needed for that purpose and must be run at least once. Alternatively, experimental data can be used if available.

IV. SELF-FORCES

The scale function $f(r/R,\theta)$ is approximately universal only if all electromagnetic forces are negligible. This includes self-forces as well as those produced externally. The self-forces vary inversely with the beam radius a_b and are therefore negligible only if a_b is not too small. But this requirement conflicts with the definition of a pencil beam, $a_b \to 0$ at injection.

To illustrate the problem, consider a cylindrical beam propagating in dense gas. The beam both ionizes the gas and deposits charge. The charge moves out radially through the beam-generated plasma and thus has little effect on the beam in steady state. However, the plasma is too resistive to fully neutralize the beam current near the z axis, and that current produces an azimuthal magnetic field which pinches the beam electrons radially and causes them to oscillate about the z axis.[16,42] Accordingly, in the absence of collisions, the mean-square radius of an initially cold beam begins to contract,

$$a_b^2(z) = a_0^2 \cos^2(k_\beta z) = a_0^2[1 - (k_\beta z)^2 + \cdots]. \tag{18}$$

Here a_0 is the initial beam radius, $k_\beta = a_b^{-1}\sqrt{I_b/I_A}$ is the betatron wave number, and $I_A = \beta\gamma mc^3/e \simeq 17\beta\gamma$ kA is the Alfven current.[42] Self-pinching can be neglected, of course, if $k_\beta R \ll 1$.

Elastic collisions, on the other hand, cause the beam to expand. In particular, in the absence of a pinch force, an initially cold beam expands according to[16,42]

$$a_b^2 \simeq a_0^2 + \frac{2z^3}{3R_{\rm el}} + \cdots. \tag{19}$$

A comparison of the last terms in Eqs. (18) and (19) suggests that self-pinched beams begin to expand once they have traveled an axial distance,

$$z > L_N \equiv \frac{I_b}{I_A} R_{\rm el}, \tag{20}$$

where L_N is the Nordsieck length.[42] If $\lambda_\beta \ll L_N \ll R_{\rm el}$, gas scattering and the pinch force nearly offset one another, and the beam radius a_b then grows slowly but exponentially with z/L_N.[16,42] Equation (1) does not apply in this self-pinched regime.

The pinch force has virtually no effect, however, if $L_N \ll R_{\rm el}$ and $k_\beta L_N \ll 1$. The latter two conditions are equivalent to

$$I_b \ll I_A,$$

$$a_0 \gg R_{\rm el}\left(\frac{I_b}{I_A}\right)^{3/2}. \tag{21}$$

Self-forces can therefore be ignored provided the beam current is not too large and the initial beam radius is not too small, and in this regime Eq. (1) is justified. For example, $I_b/I_A \simeq 3\times 10^{-4}$ for a beam injected with 1 A and 10 keV. Such a beam can therefore be represented by a series of unpinched pencil beams provided its initial radius satisfies $a_0 \geq 5\times 10^{-5} R_{\rm el}$. Smaller beams can be treated if the current is lower or the energy is higher.

V. SPATIAL RESOLUTION

The scale function $f(r/R,\theta)$ diverges at $r=0$ because the beam current density is infinite at the origin by assumption. This singularity complicates model calculations without providing any benefit. However, to model beams with a finite initial radius a_0, the function $f(r/R,\theta)$ can be averaged over a_0 without seriously compromising its utility. For example,

Downloaded 02 Oct 2008 to 132.250.158.10. Redistribution subject to AIP license or copyright; see http://jap.aip.org/jap/copyright.jsp

in the simulations that will be described later, cylindrical shells of equal thickness and length were used: $\Delta\rho=\Delta z \simeq 10^{-2}R$. The initial radius of the "pencil" beam used to compute $f(r/R,\theta)$ was two orders of magnitude smaller, $10^{-2}\Delta\rho$. Because the cell size was finite, the values obtained for $f(r/R,\theta)$ were finite, and these values are sufficient for modeling beams having initial radii of $10^{-2}R$ or greater. But to model smaller beams, $f(r/R,\theta)$ should be recomputed using smaller cells near the origin.

Although small cells can and should be used near the origin, large cells are required at large r/R to suppress particle noise. Large cells limit, however, the spatial resolution attainable, especially near the outer edge of the beam where $f(r/R,\theta)$ falls rapidly to zero. That region is difficult to model accurately.

VI. OTHER ISSUES

The beam range can be specified in different ways,[21,43] and two definitions have been given thus far. The inelastic range R is the mean distance traveled before the beam electrons run out of energy, while the elastic range R_{el} is the distance needed for the electrons to isotropize. The elastic cross sections are proportional to the square of the nuclear charge Z_k, whereas the sum of the inelastic cross sections is roughly proportional to the number Z_k of orbital electrons. Therefore R/R_{el} varies almost linearly with Z_k, so beams broaden more in high-Z materials than in low-Z materials. In addition, random-walk theory suggests that the mean (axial) penetration depth satisfies

$$R_z \simeq \sqrt{R_{\mathrm{el}}R} \simeq \chi\frac{R}{\sqrt{Z_k}}, \tag{22}$$

where $\chi\sim 1$. Calculations by Tabata *et al.*[43] indicate that $\chi \simeq 2.6$ for $6<Z_k\leq 92$ at initial beam energies below 1 MeV. In air the elastic and inelastic ranges are comparable, and $R_z\simeq R$. Beams thus expand radially almost as much as axially, as shown in Fig. 1.

This work has focused on energy deposition because that is the primary parameter of interest for most applications. However, other beam parameters can be determined. For example, the fraction of beam electrons passing through a plane located a distance z from the source is a function mainly[20] of z/R. Given this function, the initial energy of a beam can be determined by placing foils of various thicknesses in front of the beam and measuring the current detected on the other side. We have successfully used this technique to calibrate high-voltage beams in unpublished experiments.

The self-similar model applies, of course, only after the electron energy distribution has equilibrated. The equilibration time τ is approximately equal to the inelastic range R divided by the mean speed of the beam electrons. This estimate is consistent with calculations performed using a Boltzmann code.[18] For example, a 100 keV beam has a range $R\simeq 10$ cm in atmospheric air, so $\tau\simeq 1$ ns. Equation (1) is then justified a few nanoseconds after injection.

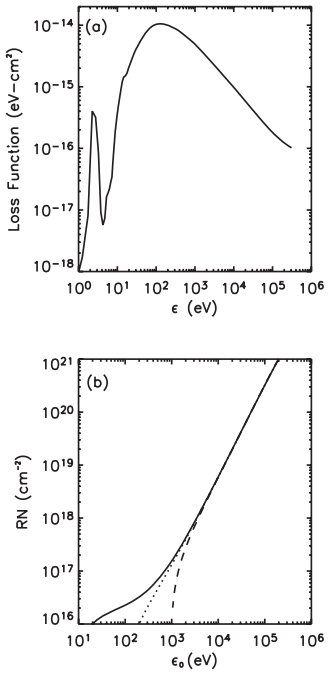

FIG. 2. (a) Reduced energy-loss function $N^{-1}(d\varepsilon/ds)$ as a function of electron energy ε in air. (b) Reduced range $NR(\varepsilon_0,\varepsilon_1)$ as a function of initial beam energy ε_0 for ε_1 equal to 1 keV (dashed), 100 eV (dotted), and 10 eV (solid).

VII. SIMULATION RESULTS

The PLUME code was run at various gas densities N for initial energies ε_0 between 0.5 and 200 keV. The scaling with N was straightforward and will not be discussed further. The scaling with energy was determined by first computing

$$R(\varepsilon_0,\varepsilon_1)=\int_{\varepsilon_1}^{\varepsilon_0} d\varepsilon(d\varepsilon/ds)^{-1}. \tag{23}$$

Here ε_1 is a cutoff separate from $\varepsilon_{\min}$ and $d\varepsilon/ds=\Sigma N_k E_{jk}\sigma_{jk}$ is the loss function. Figure 2 shows normalized plots of $d\varepsilon/ds$ and $R(\varepsilon_0,\varepsilon_1)$ for various values of ε_1. These plots indicate that $R(\varepsilon_0,\varepsilon_1)$ reaches a minimum at $\varepsilon_1 \simeq 100$ eV, where $d\varepsilon/ds$ peaks. Since elastic collisions strongly confine electrons below 100 eV, the effective inelastic range lies along the nearly straight-line portion of the curve in Fig. 2(b). That portion can be fit by

$$RN \simeq 5.3\times 10^{11}\varepsilon_0^{7/4}, \tag{24}$$

where R is in cm, N is in cm^{-3}, and ε_0 is in eV. This fit agrees well with optical emission measurements by Grűn[26] and others[27,28] and with earlier Monte Carlo calculations.[21,22,38] Note that Eq. (24) is a better fit than Eq. (14).

After deriving Eq. (24), we used Eq. (1) to compute the scale function $f(r/R,\theta)$ from the energy deposited in each cell. Representative plots of $f(r/R,\theta)$ are shown in Fig. 3 along cords taken at $\rho/R=0,0.3,0.6,0.8$ for initial beam energies between 1 and 200 keV, where $\rho=(r^2-z^2)^{1/2}$. Over 4×10^5 beam electrons were injected at 200 keV and over 10^6 electrons at the lower energies; the number of daughter electrons was much larger, of course. As is evident, the solutions for $f(r/R,\theta)$ overlap to within $\pm 15\%$ for $\varepsilon_0\geq 5$ keV and $r/R<1$. The differences increase below 5 keV and also at

Downloaded 02 Oct 2008 to 132.250.158.10. Redistribution subject to AIP license or copyright; see http://jap.aip.org/jap/copyright.jsp

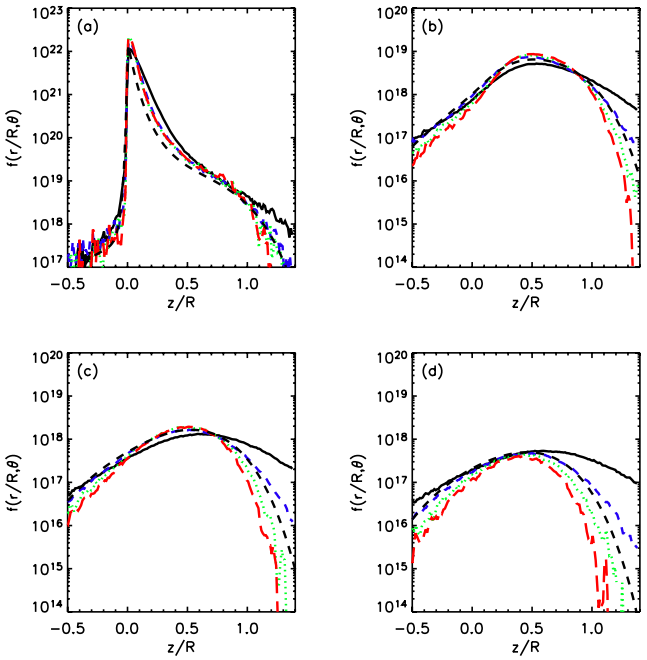

FIG. 3. (Color online) Scale function $f(r/R,\theta)$ at (a) $\rho/R=0$, (b) $\rho/R=0.3$, (c) $\rho/R=0.6$, and (d) $\rho/R=0.8$ for initial energies of 1 keV (solid black), 5 keV (small blue dashes), 50 keV (green dots), and 200 keV (large red dashes). The smooth black-dashed curve shows the fit given by Eqs. (25) and (26). Note that the curves do not truly overlap, especially at large r/R.

$r/R \geq 1$, where few high-energy electrons are present. The presence of electrons at $r>R$ reflects range straggling, and in those regions the statistical fluctuations are large. While the disparities could possibly be reduced by modifying Eq. (24), they cannot be eliminated because the coefficients for scattering and energy loss are not truly proportional. Note too that the variations seen at high energy for $r/R \leq 1$ are generally less than the uncertainties in the cross sections.

In the backscattered direction $z<0$, the function $f(r/R,\theta)$ drops precipitously but the curves in Fig. 3 continue to overlap. Few electrons are found in this region because backscattering is weak. However, while reflection from a boundary is similarly weak, it is *not* self-similar. For example, if an absorbing boundary is placed at $z=0$, the transmission fraction[20] in the forward direction remains a function mainly of z/R, as discussed earlier. But the number of electrons reflected from the boundary varies with ε_0 and ultimately approaches zero at high energy.[20] The reflection fraction varies because high-energy electrons suffer more collisions on average and are thus less likely to escape than low-energy electrons.

Included in Fig. 3 is an algebraic fit for $f(r/R,\theta)$. Because $f(r/R,\theta)$ varies by many orders of magnitude, the function $g(x,\theta) \equiv \ln[f(x,\theta)]$ was fit instead; here $x=r/R$. Unlike photons, beam electrons are not destroyed by collisions and thus do not obey the Beer-Lambert law commonly assumed in spectroscopic analyses.[44,45] Instead the electrons gradually lose energy and scatter. Moreover, because energy loss and scattering both depend on the instantaneous energy, the two processes cannot be treated separately.[20] Accordingly, $g(x,\theta)$ is highly nonlinear in x as well as θ, as is evident from the fit finally obtained,

$$g(x,\theta) = \{[705.5 - B(\theta)]e^{-\alpha(\theta)x} + B(\theta)\chi(x,\theta)\}q(x,\theta), \tag{25}$$

where

$$B(\theta) = 16.509 - 1.1794\cos(\theta/2) + 6.4294\cos^2(\theta/2) - 11.0\cos^3(\theta/2) + 6.979\cos^4(\theta/2),$$

$$\alpha(\theta) = 29.84 + 10.178\cos^2(\theta/2) - 117.11\cos^4(\theta/2) + 459.98\cos^6(\theta/2) - 693.6\cos^8(\theta/2) + 315.72\cos^{10}(\theta/2),$$

$$\chi(x,\theta) = \max\left\{1 - \frac{2}{1+e^{-\Phi(\theta)(x-2.16)}}, 0\right\},$$

$$q(x,\theta) = \max\left\{1 - \frac{2}{1+e^{-60[x-x_c(\theta)]}}, 0\right\},$$

$$\Phi(\theta) = 1.983 + 1.22\cos^2(\theta/2),$$

$$x_c(\theta) = 0.45 + 2.339\cos(\theta/2) - 1.0792\cos^2(\theta/2). \tag{26}$$

The functional form of Eqs. (25) and (26) is largely arbitrary and only partially reflects the underlying physics. The fit is therefore neither unique nor optimal, and more accurate and simpler fits are presumably possible. Note too that $g(x,\theta)$ remains finite as $x \to 0$. Nevertheless, the fit is fairly good over many orders of magnitude, and the numerical results demonstrate that Eq. (1) is well justified over most of the beam range for initial energies above several keV. Given the mean energy ε_{jk} per state, the ionization and excitation rates can be estimated equally easily.

To assess the role of the daughter electrons, the code was reconfigured to follow the beam electrons only, with ionization treated solely as an energy loss. Shown in Fig. 4 are plots of the normalized energy deposited on axis by all electrons (solid) and by beam electrons only (dots) for initial beam energies of 1 and 10 keV. These results demonstrate that the daughter electrons broaden the deposition significantly only at initial energies below 10 keV. Eliminating the daughter electrons greatly reduces the run time, especially at high energy.

VIII. CONCLUSION

Previous studies of light emission have shown that electron beams behave nearly self-similarly when scaled to the beam range R. However, the physical basis for this behavior was never fully developed or formulated. In this work we derived scaling relationships for energy loss and scattering and found that both processes depend similarly on density and energy above 1 keV. Accordingly, the behavior of an initially cold pencil beam is approximately self-similar for initial beam energies above several keV. Since a warm and broad beam can always be represented by a series of cold pencil beams, the energy deposited by more general beams can be easily estimated.

To prove and quantify the above conjecture, we constructed a particle code for modeling beams in air. Unlike

Downloaded 02 Oct 2008 to 132.250.158.10. Redistribution subject to AIP license or copyright; see http://jap.aip.org/jap/copyright.jsp

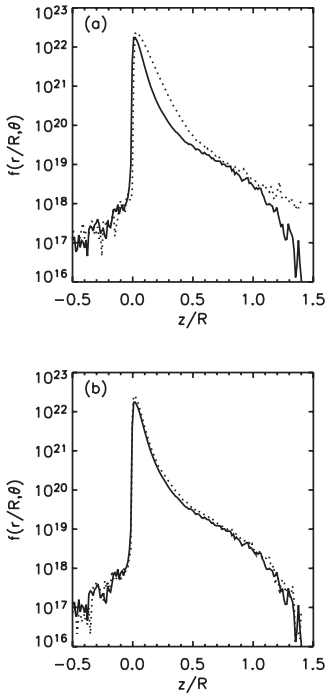

FIG. 4. On-axis scaled energy deposition with (solid curve) and without (dots) daughter electrons for initial energies of (a) 1 keV and (b) 10 keV.

more generic codes, the PLUME code treats all collisions individually using discrete cross sections for scattering, excitation, and ionization. The code follows both the beam electrons and the daughter electrons created by ionization, and it gives both the energy deposited and the number of ions and excited molecules created at each point in space. As expected, the individual production rates are nearly directly proportional to the energy being deposited. The code results were used to obtain an algebraic approximation for R, and the energy deposited was then rescaled to R using that expression. The scaled results overlapped to within $\pm 15\%$ over most of the beam range for initial beam energies between 5 and 200 keV, the maximum energy studied. An algebraic fit to the scaled behavior was obtained, and with that fit one can easily estimate the production and energy-deposition rates for more general beams. While the particle code can provide the same information, an algebraic formula is far easier and faster to use, especially for beams that are noncylindrical and inherently three-dimensional. Modeling complex beams over a wide range of conditions is thus simpler algebraically than numerically.

The algebraic formulation is only approximate because the mean free paths for energy loss and scattering are not truly proportional. The error is largest at low energy and increases beyond the beam range. These disparities could potentially be reduced by revising the formula for R and/or by using different basis functions for $f(r/R,\theta)$. Alternatively, the weak dependence on energy could be incorporated as a higher-order correction. Those refinements are left for future studies.

ACKNOWLEDGMENTS

This work was supported by the Office of Naval Research.

[1]U. Fano, Phys. Rev. **92**, 328 (1953).
[2]M. Inokuti, in *Applied Atomic Collisions Physics*, edited by S. Datz (Academic, New York, 1983), Vol. 4.
[3]A. Dalgarno and G. Lejeune, Planet. Space Sci. **19**, 1653 (1971).
[4]M. H. Rees, Planet. Space Sci. **11**, 1209 (1963).
[5]P. S. Ganas and A. E. S. Green, J. Quant. Spectrosc. Radiat. Transf. **25**, 265 (1981).
[6]S. D. Rockwood, Phys. Rev. A **8**, 2348 (1973).
[7]J. Bretagne, J. Godart, and V. Puech, J. Phys. D **15**, 2205 (1982).
[8]F. Kannari and W. D. Kimura, J. Appl. Phys. **63**, 4377 (1988).
[9]F. Hegeler, D. V. Rose, M. C. Myers, J. D. Sethian, J. L. Giuliani, M. F. Wolford, and M. Friedman, Phys. Plasmas **11**, 5010 (2004).
[10]B. M. Penetrante, M. C. Hsiao, J. N. Bardsley, B. T. Merritt, G. E. Vogtlin, A. Kuthi, C. P. Burkhart, and J. R. Bayless, Plasma Sources Sci. Technol. **6**, 251 (1997).
[11]L. A. Gochberg, Prog. Aerosp. Sci. **33**, 431 (1997).
[12]M. J. Kushner, W. Z. Collison, and D. N. Ruzic, J. Vac. Sci. Technol. A **14**, 2094 (1996).
[13]W. M. Manheimer, R. F. Fernsler, M. Lampe, and R. A. Meger, Plasma Sources Sci. Technol. **9**, 370 (2000).
[14]A. V. Vasenkov, J. Phys. D **32**, 240 (1999).
[15]R. F. Fernsler, W. M. Manheimer, R. A. Meger, J. Mathew, D. P. Murphy, R. E. Pechacek, and J. A. Gregor, Phys. Plasmas **5**, 2137 (1998).
[16]R. F. Fernsler, R. F. Hubbard, and M. Lampe, J. Appl. Phys. **75**, 3278 (1994).
[17]L. V. Spencer, Phys. Rev. **98**, 1597 (1955).
[18]S. P. Slinker, A. W. Ali, and R. D. Taylor, J. Appl. Phys. **67**, 679 (1990).
[19]I. Kawrakow and A. F. Bielajew, Nucl. Instrum. Methods Phys. Res. B **142**, 253 (1998).
[20]S. M. Seltzer and M. J. Berger, Nucl. Instrum. Methods **119**, 157 (1974).
[21]S. Valkealahti, J. Schou, and R. M. Nieminen, J. Appl. Phys. **65**, 2258 (1989).
[22]A. Morozov, R. Krűcken, and A. Ulrich, J. Appl. Phys. **100**, 093305 (2006).
[23]A. V. Vasenkov, Phys. Rev. E **57**, 2212 (1998).
[24]H. Bethe, Ann. Phys. **5**, 325 (1930).
[25]J. D. Jackson, *Classical Electrodynamics* (Wiley, New York, 1967).
[26]A. E. Z. Grűn, Z. Naturforsch. A **12**, 89 (1957).
[27]A. Cohn and G. Caledonia, J. Appl. Phys. **41**, 3767 (1970).
[28]J. L. Barrett and P. B. Hays, J. Chem. Phys. **64**, 743 (1976).
[29]H. W. Lewis, Phys. Rev. **78**, 526 (1950).
[30]G. Moliere, Z. Naturforsch. A **3**, 78 (1948).
[31]R. Mayol and F. Salvat, At. Data Nucl. Data Tables **65**, 55 (1997).
[32]C. H. Jackman and A. E. S. Green, J. Geophys. Res. **84**, 2715 (1979).
[33]A. Okhrimovskyy, A. Bogaerts, and R. Gijbels, Phys. Rev. E **65**, 037402 (2002).
[34]Y. Itikawa, J. Phys. Chem. Ref. Data **35**, 31 (2006).
[35]Y. Itikawa, A. Ichimura, K. Onada, K. Sakimoto, K. Takayanagi, Y. Hatano, M. Hayshi, H. Nishimura, and S. Tsurubuchi, J. Phys. Chem. Ref. Data **18**, 23 (1989).
[36]H. S. Porter, C. H. Jackman, and A. E. S. Green, J. Chem. Phys. **65**, 154 (1976).
[37]S. P. Slinker, R. D. Taylor, and A. W. Ali, J. Appl. Phys. **63**, 1 (1988).
[38]See, for example, "Stopping powers for electrons and positrons," International Commission of Radiation Units and Measurements Report No. 37, 1984.
[39]C. B. Opal, E. C. Beaty, and W. K. Peterson, At. Data **4**, 209 (1972).
[40]S. T. Manson, L. H. Toburen, D. H. Madison, and N. Stolterfoht, Phys. Rev. A **12**, 60 (1975).
[41]E. J. Williams, Proc. R. Soc. London, Ser. A **130**, 328 (1931).
[42]E. P. Lee, Phys. Fluids **19**, 60 (1976).
[43]T. Tabata, P. Andreo, K. Shinoda, and R. Ito, Nucl. Instrum. Methods Phys. Res. B **95**, 289 (1995).
[44]Y. Tsuchiya, Phys. Med. Biol. **46**, 2067 (2001).
[45]A. Sassaroli and S. Fantini, Phys. Med. Biol. **49**, N255 (2004).

Downloaded 02 Oct 2008 to 132.250.158.10. Redistribution subject to AIP license or copyright; see http://jap.aip.org/jap/copyright.jsp